published online in EPJ Direct
http://www.springeronline.com/sgw/cda/frontpage/0,10735,5-40213-12-105188-0,00.html

Prospects for the Search for a Standard Model Higgs Boson in ATLAS using Vector Boson Fusion

S.Asai[8], G.Azuelos[5] C.Buttar[7], V.Cavasinni[6], D.Costanzo[6,a], K.Cranmer[9], R.Harper[7], K. Jakobs[4], J.Kanzaki[3], M.Klute[1], R.Mazini[5], B.Mellado[9], W.Quayle[9], E.Richter-Wąs[2], T.Takemoto[3], I.Vivarelli[6], Sau Lan Wu[9]

[1] Physikalisches Institut, Universität Bonn, Germany.
[2] CERN, Geneva, Switzerland[b] and Inst. of Nuclear Physics, Cracow, Poland.
[3] High Energy Research Organisation (KEK), IPNS, Japan.
[4] Institut für Physik, Universität Mainz, Germany.
[5] University of Montreal, Canada.
[6] INFN and University of Pisa, Italy.
[7] Dept. of Physics and Astronomy, University of Sheffield, UK.
[8] University of Tokio, Tokio, Japan.
[9] University of Wisconsin-Madison, Wisconsin, USA.

Received: 24 April 2003 / Published online: 30 July 2003

Abstract. The potential for the discovery of a Standard Model Higgs boson in the mass range $m_H < 2m_Z$ in the vector boson fusion mode has been studied for the ATLAS experiment at the LHC. The characteristic signatures of additional jets in the forward regions of the detector and of low jet activity in the central region allow for an efficient background rejection. Analyses for the $H \to WW^{(*)}$ and $H \to \tau\tau$ decay modes have been performed using a realistic simulation of the expected detector performance. The results obtained demonstrate the large discovery potential in the $H \to WW^{(*)}$ decay channel and the sensitivity to Higgs boson decays into τ-pairs in the low-mass region around 120 GeV/c^2.

1 Introduction

The search for the Higgs boson is one of the primary tasks of the experiments at the *Large Hadron Collider* (LHC). It has been established by many studies [1,2] that a Standard Model Higgs boson can be discovered with high significance over the full mass range of interest, from the lower limit set by the LEP experiments of 114.1 GeV/c^2 [3] up to about 1 TeV/c^2.

At the LHC, the production cross-section for a Standard Model Higgs boson is dominated by gluon-gluon fusion. The second largest cross-section comes from the fusion of vector bosons radiated from initial-state quarks. The relative contributions of the two processes depend on the Higgs boson mass. For $m_H < 2m_Z$, vector boson fusion amounts in leading order to about 20% of the total production cross-section and becomes more important with increasing mass. However, for this production mode, additional event characteristics can be exploited to suppress the large backgrounds. The Higgs boson is accompanied by two jets in the forward regions of the detector, originating from the initial quarks that emit the vector bosons. In addition, central jet activity is suppressed due to the lack of color exchange between the quarks. This is in contrast to most background processes, where there is color flow in the t-channel. Therefore jet tagging in the forward region of the detector together and a veto of jet activity in the central region are useful tools to enhance the signal-to-background ratio. These techniques have been considered already in the studies performed for heavy Higgs bosons [1].

The observation of the Standard Model Higgs boson at the LHC in the vector boson fusion channels in the intermediate mass range was first discussed in Refs. [4] and [5] for the $H \to \gamma\gamma$ and $H \to WW^{(*)}$ decay modes and in Ref. [6] for the $H \to \tau\tau$ decay mode. The latter is particularly interesting for a measurement of the Higgs boson coupling to fermions in the low-mass region, *i.e.,* $m_H < 140$ GeV/c^2, since beyond the $b\overline{b}$ decay mode, no other direct fermion decay mode is accessible at the LHC.

In the present study, the analyses for the $WW^{(*)}$ and $\tau\tau$ decay modes have been performed using realistic simulations of the expected performance of the ATLAS detector at the LHC, including forward jet tagging. The performance is addressed at low LHC luminosity, *i.e.,* $\mathcal{L} = 10^{33}$ cm^{-2}sec^{-1}, and the discovery potential is evaluated for an integrated luminosity up to 30 fb^{-1}, which is expected to be reached during the first few years of operation.

[a] Now at LBNL, Berkeley, USA
[b] On leave of absence from Jagellonian University, Cracow, Poland

In Section 2, the cross-sections and the event generation for the signal and for various background processes are discussed. Important experimental issues in the search for vector boson fusion processes at the LHC are addressed in Section 3. General signal selection criteria are presented in Section 4, before the detailed analyses for the $H \to WW^{(*)}$ and for the $H \to \tau\tau$ decay modes are considered in Sections 5 and 6. The ATLAS Higgs boson discovery potential in the low-mass region is summarized in Section 7.

2 Signal and Backgrounds

The cross-sections for the vector boson fusion process have been calculated using the programme VV2H [7]. The results are given in Table 1 as a function of the Higgs boson mass. Although next-to-leading order calculations are available [8] and have been found to increase the cross-section by $\sim 10\%$, leading order cross-sections have been used. The main reason for this approach is the consistency with the background estimates, for which NLO cross-section calculations are not available for all relevant processes. Since the NLO correction for the signal is relatively small, the significance might be overestimated if the NLO corrections for the backgrounds are large. The products of the cross-sections multiplied by the branching ratios of the Higgs boson into WW and $\tau\tau$, which have been calculated using the programme HDECAY [9], are also included in Table 1.

The following decay chains have been considered in the analysis:

- $qqH \to qq\ W^+W^- \to\ qq\ \ell^+\nu\ \ell^-\nu$
- $qqH \to qq\ W^+W^- \to\ qq\ \ell^\pm\nu\ jet\ jet$
- $qqH \to qq\ \tau^+\tau^- \quad \to\ qq\ \ell^+\nu\nu\ \ell^-\nu\nu$
- $qqH \to qq\ \tau^+\tau^- \quad \to\ qq\ \ell^\pm\nu\nu\ \ \ had\ \nu.$

All final states consist of at least one high-P_T lepton, missing transverse momentum and two jets in the forward regions of the detector. The following background processes are common to all channels considered:

- *$t\bar{t}$ and Wt production:*
  The dominant background contribution comes from $t\bar{t}$ production. The production cross-section is large and the leptonic decays (into e, μ and τ) of the W's, produced in the $t \to Wb$ decays, lead to a signature similar to the signal. Due to the appearence of two b-jets that can mimic the forward jet tags, $t\bar{t}$ events contribute to the background already at leading order.
  Another important background results from single-top production in association with a W boson, where the leptons result from the W and the top quark decay.
- *QCD WW + jet production:*
  The continuum production of W pairs in association with two or more jets is another background. The diagrams referred to as QCD-WW production involve color exchange between the initial and final partons.
- *Electroweak WW + jet production:*
  Pairs of W bosons may also be produced in an electroweak (EW) process via vector boson exchange. Although this background has a much lower cross-section than the QCD-WW production, it shows similar characteristics to the signal process. The electroweak bosons exchanged in the t-channel are radiated off the initial quarks and no color flow is exchanged. Due to this similarity to the signal process, the rejection of this particular background is expected to be much harder than for the QCD-type backgrounds.
- *QCD γ^*/Z + jet production:*
  The Drell-Yan γ^*/Z + jet production has a large cross-section at the LHC. For electron and muon pairs in the final state, the main discriminating variable between signal and background is the missing transverse momentum. In addition, the Z-resonance peak can be vetoed by applying a cut on the invariant mass of the same flavour di-lepton pair.
  Tau pairs in the final state from $\gamma^*/Z \to \tau^+\tau^-$ represent a potentially serious background for the Higgs search in the $\tau\tau$ decay mode. If both τ-leptons decay leptonically, this process also contributes to the $H \to WW^{(*)} \to \ell\nu\ell\nu$ search.
  In addition to Drell-Yan, processes involving gluon splitting in the initial state $qg \to qg\tau\tau, gg \to q\bar{q}\tau\tau$ or quark scattering, dominated by t-channel gluon exchange with Z or γ bremsstrahlung, contribute to this background process.
- *Electroweak $\tau\tau$ + jet production:*
  Tau pairs can also be produced in an electroweak process, via a t-channel weak boson exchange. As in the case of the electroweak WW production, a larger acceptance compensates the smaller production cross-section.
- *ZZ production:*
  An additional background comes from ZZ production. There is a contribution where one Z decays into an $ee/\mu\mu$ pair and the other hadronically, leading to jets. Another contribution results from ZZ events where the second Z decays into a pair of neutrinos and jets are produced from additional QCD radiation.

An additional background that has not been considered in detail can arise from $b\bar{b}$ production, which has a huge cross-section at the LHC. Previous studies [11] have shown that requiring two high-P_T isolated leptons in association with P_T^{miss} and/or angular cuts on the leptons will suppress this background well below the level of the other backgrounds listed above.

The signal process and all background processes except the single top, the electroweak WW and $\tau\tau$ production have been generated using the PYTHIA 6.1 Monte Carlo event generator [12]. Initial- and final-state radiation (ISR and FSR) and fragmentation, as well as multiple interactions, have been switched on, thereby allowing for a study of the jet activity in the central detector region due to radiation. The CTEQ5L parametrization [10] of the parton distribution functions has been used in the generation of all signal and background processes. To take the spin

m_H	($\mathrm{GeV/c^2}$)	120	130	140	150	160	170	180	190
$\sigma(qqH)$	(pb)	4.36	4.04	3.72	3.46	3.22	3.06	2.82	2.64
$\sigma \cdot BR(H \to WW^{(*)})$	(fb)	531	1127	1785	2370	2955	2959	2620	2054
$\sigma \cdot BR(H \to \tau\tau)$	(fb)	304	223	135	64.4	11.9	2.8	1.6	1.0

Table 1. *Total vector boson fusion production cross-sections $\sigma(qqH)$ and $\sigma \cdot BR(H \to WW^{(*)})$ and $\sigma \cdot BR(H \to \tau\tau)$ as a function of the Higgs boson mass. The cross-sections have been computed using the CTEQ5L structure function parametrization [10].*

process	P_T-cutoff	cross-section
$\gamma^*/Z\ + jets$, $\gamma^*/Z \to \ell\ell$	> 10 GeV/c	5227 pb
$t\bar{t}$		55.0 pb
QCD $WW + jets$		16.7 pb
$qg \to Wt$		4.8 pb
EW $\tau\tau + jets$		170.8 fb
EW $WW + jets$		81.6 fb

Table 2. *cross-sections times leptonic branching ratios ($W \to \ell\nu$, $\ell = e, \mu$ and τ) for the major background processes.*

correlations properly into account, tau decays have been modelled using the TAUOLA decay library [13]. The two electroweak processes, which are not included in PYTHIA, and the QCD $\gamma^*/Z + jet$ production have been generated by interfacing the parton-level generation of Ref. [5] to PYTHIA, which was then used to perform the parton showering, including initial- and final-state radiation [14]. The single-top background has been generated using the Monte Carlo programme of Ref. [15].

Since the $t\bar{t}$ and the $\gamma^*/Z + jet$ with $Z \to \tau\tau$ backgrounds are the dominant backgrounds for the $WW^{(*)}$ and $\tau\tau$ decay modes respectively, these backgrounds have been generated also using explicit tree-level matrix element calculations for $t\bar{t}$ + 0, 1, and 2 jets[1] and Z + 2 jets. The latter process has also been generated using the *COMPHEP* Monte Carlo generator [16].

A summary of the major background processes and the relevant cross-sections multiplied by the branching ratios $BR(W \to \ell\nu)$ and $BR(Z \to \ell\ell)$, where $\ell = e, \mu$ and τ are listed in Table 2.

ATLFAST [17], the package for the fast simulation of the ATLAS detector, has been used to perform the detector simulation for all processes considered. This simulation provides a parametrized response of the crucial detector performance figures, based on detailed GEANT simulations [1].

[1] The matrix element calculations were provided by the authors of Ref. [5]

3 Experimental Issues

In this section, several experimental issues that are common to all vector boson fusion analyses are discussed. Among them are the questions of the trigger, the forward jet tagging and the central jet veto.

3.1 Trigger aspects

All channels considered have leptons (e or μ) in the final state and can be triggered by either the single- or the di-lepton trigger. The hardest trigger requirements are set by the $\tau\tau$ decay mode, where in the di-lepton channel low P_T-thresholds for the reconstructed leptons are needed to keep the acceptance at a high level. Assuming the ATLAS trigger thresholds [18], high trigger efficiency can be reached for a single electron or muon for P_T values above 25 GeV/c or 20 GeV/c respectively. The ATLAS trigger acceptance covers the region $|\eta| < 2.5$ for electrons and $|\eta| < 2.2$ for muons. The P_T-threshold values for the lepton pair triggers are 15 GeV/c (for ee) and 10 GeV/c (for $\mu\mu$). For the mixed mode (e, μ), it is assumed that each lepton passes the respective threshold of 10 GeV/c for muons and 15 GeV/c for electrons or that at least one of them passes the higher thresholds of the single-lepton trigger. Lepton-hadron $\tau\tau$ final states can be triggered via the single-lepton trigger or via the hadronic tau + P_T^{miss} trigger.

3.2 Lepton Identification

The reconstruction of electrons and muons has been studied in detailed detector simulations [1] including the effects of pileup. Based on these studies, the efficiency for the reconstruction of electrons or muons in the pseudorapidity range of the ATLAS Inner Detector, $|\eta| < 2.5$, is taken to be 90%.

It is further assumed that hadronically decaying taus can be identified over the same range of pseudorapidity. Important ingredients in the tau identification [19] are the profile of the energy deposition in the calorimeter and the number of tracks with a transverse momentum above 1 GeV/c pointing to the calorimeter cluster. The tau reconstruction efficiency is correlated with the rejection against jets [1,19]. In the present study, an efficiency of 50% for hadronic tau decays is assumed. This leads to a typical rejection [1] of about 100 for jets with a P_T of 40 GeV/c.

3.3 Jet Tagging

From the production process it is expected that the two tag jets are reconstructed with a sizeable P_T in opposite hemispheres and have a large separation in pseudorapidity. Without further hard initial- or final-state radiation, the transverse momentum of the tagging jets should be balanced by the transverse momentum of the Higgs boson.

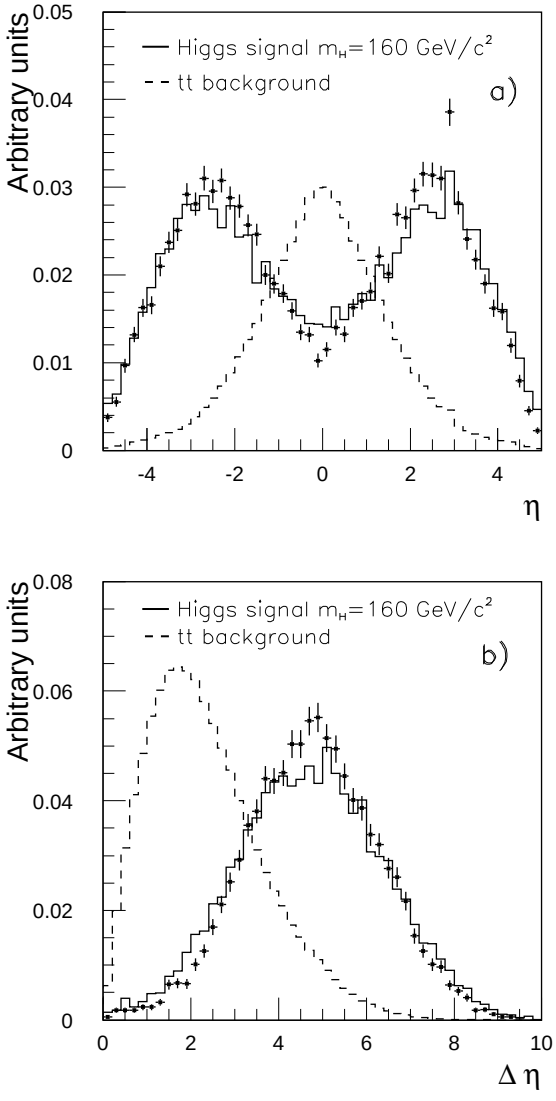

Fig. 1. *a) Pseudorapidity distribution of the tag jets in signal events with $m_H = 160$ GeV/c^2 and for $t\bar{t}$ background events. The full histograms show the distributions at parton level, the dots represent the reconstructed distributions, after the tagging algorithm has been applied. The corresponding distributions for jets identified as tag jets in $t\bar{t}$ events are superimposed as dashed histograms. All distributions are normalized to unity. b) Separation $\Delta\eta$ between the tag jets for the same types of events.*

In the present study, the two tag jets are searched for over the full calorimeter coverage of the ATLAS detector ($|\eta| < 4.9$). For all jets, a calibration has been applied which corrects the jet energy on average back to the original parton energy. After the calibration, the jets with the highest P_T in the positive and negative regions of pseudorapidity are taken to be the tag jet candidates. Studies have shown [20] that this choice of the tag jets has a high efficiency for correctly identifying the tag jets.

The pseudorapidity distribution and the separation $\Delta\eta$ between the two tag jets, as found from the parton-level information, is shown in Fig. 1 for signal events with $m_H = 160$ GeV/c^2 (full histogram). Using the tagging algorithm described above, good agreement is found between the parton level and the reconstructed information, which is represented by the dots in the figure. Due to the opposite hemisphere requirement, a small bias is found for jets with a small pseudorapidity separation; however, this does not affect the final result. Also superimposed onto this figure are the corresponding distributions for tag jets as reconstructed in $t\bar{t}$ background events. A comparison between the distribution for signal and background events clearly suggests that a large pseudorapidity separation should be used for the discrimination between signal and QCD-type backgrounds.

In order to address the question how well these jets can be identified at the LHC in the presence of pileup, a full GEANT simulation of the performance of the ATLAS detector has been performed [21]. This study has demonstrated that tag jets can be reliably reconstructed in the ATLAS detector. The efficiency for reconstructing a tag jet in signal events with P_T above 20 GeV/c (originating from a parton with $P_T > 20$ GeV/c) is shown in Fig. 2a as a function of pseudorapidity η. The fast simulation package of the ATLAS detector provides a sufficiently good description of the tagging efficiency. Differences between the fast and full simulation have been found in the transition regions between different calorimeters and at very forward rapidities. These differences have been parametrized as a function of P_T and η and have been used to correct the fast simulation results accordingly [21].

3.4 Jet-Veto Efficiencies

As pointed out above, a veto against jets in the central region will be an important tool to suppress QCD backgrounds. At the LHC, jets in the central region can be produced also by pileup events. In the full simulation study [21], it has been found that after applying a threshold cut on the calorimeter cell energies of 0.2 GeV at low and 1.0 GeV at high luminosity, the fake jets from pileup events can be kept at a low level, provided that P_T thresholds of 20 GeV/c at low and 30 GeV/c at high luminosity are used for the jet definition. The results of this study are presented in Fig. 2b, where the efficiency to find a jet from pileup events in different intervals of central rapidity is shown as a function of the jet P_T-threshold for low and high luminosity. This behaviour demonstrates that at

high luminosity, a jet P_T-threshold of 30 GeV/c or higher should be used.

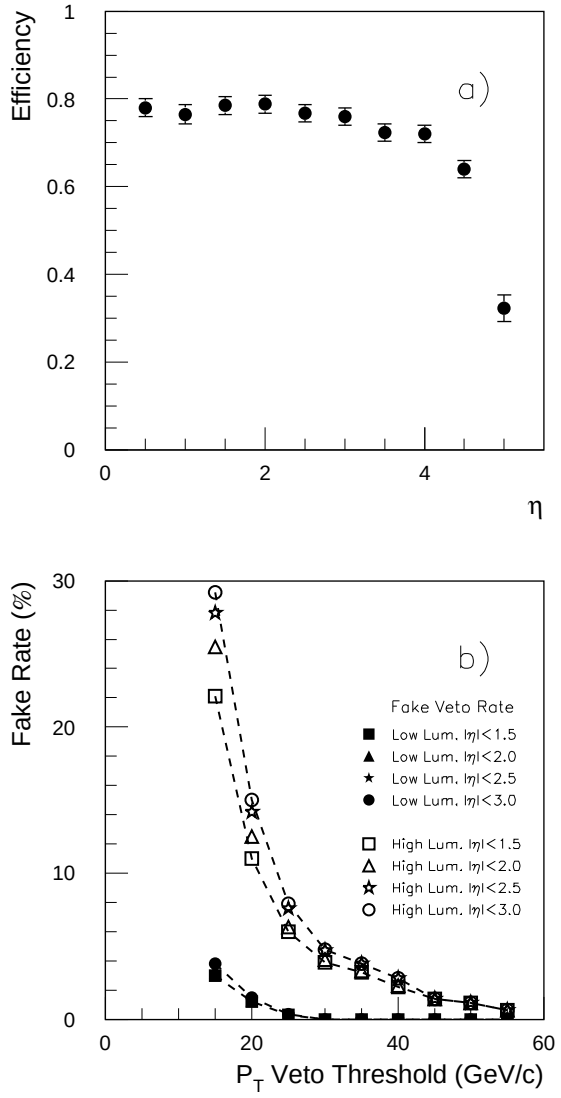

Fig. 2. *a) Efficiency for reconstructing a tag jet with $P_T >$ 20 GeV/c which originates from a parton with $P_T > 20$ GeV/c as a function of pseudorapidity η of the parton. b) Probability for finding at least one jet from pileup events in central rapidity intervals in the ATLAS detector as a function of the P_T value used in the jet definition. The dashed curves connect the points for pseudorapidity itervals $|\eta| < 1.5$ and $|\eta| < 3.0$ for low and high LHC luminosities.*

4 Signal Selection Criteria

Similar signal characteristics and reconstruction methods are exploited in the various channels considered. Common features are discussed in the following:

– *Lepton Cuts:*
A characteristic feature of the $WW^{(*)}$ decay channel is the anti-correlation of the W spins from the decay of the scalar Higgs boson [22]. Since the W^+ and W^- have opposite spins, the lepton and anti-lepton tend to be emitted in the same direction. A series of cuts is performed on the angular separation of the charged leptons, namely the azimuthal angle $\Delta\phi_{\ell\ell}$ between the lepton directions, the cosine of the polar opening angle $\cos\theta_{\ell\ell}$ and the separation in $\eta-\phi$ space $\Delta R_{\ell\ell}$. Since in the rest frame of the Higgs boson, the di-lepton system and the neutrino system are emitted back-to-back with equal energy, the invariant mass of the visible leptons, $M_{\ell\ell}$, is limited to $\sim m_H/2$. A cut on $M_{\ell\ell}$ can therefore be applied. Finally, cuts on the maximum lepton transverse momentum can be applied to reject background events without a significant loss of signal efficiency. Distributions for the variables $\Delta\phi_{\ell\ell}$ and $M_{\ell\ell}$ are shown in Fig. 3 for signal events with $m_H = 160$ GeV/c^2 and for events from several background sources.

– *Tag jets:*
The two tag jets are required to pass P_T-thresholds and to have a minimum separation in pseudorapidity $\Delta\eta_{tags} = \eta_{tag}^{max} - \eta_{tag}^{min}$. In addition, it is required that the identified leptons be reconstructed in the central region of the detector and lie in the pseudorapidity gap spanned by the two tag jets. Tag jets identified in QCD processes typically have smaller invariant jet-jet masses than those identified in electroweak processes. Therefore, the invariant mass m_{jj} of the tagged jets provides a selection criterion for the signal process.
If no hard initial- or final-state gluons are radiated, it is also expected that the transverse momentum of the Higgs boson will be balanced by the transverse momentum of the two tag jets. This behaviour is illustrated in Fig. 4, where the modulus of the vector

$$\boldsymbol{P}_T^{tot} = \boldsymbol{P}_T^{\ell,1} + \boldsymbol{P}_T^{\ell,2} + \boldsymbol{P}_T^{miss} + \boldsymbol{P}_T^{j,1} + \boldsymbol{P}_T^{j,2}$$

is shown for $H \to WW^{(*)} \to \ell\nu\ell\nu$ signal events and for $t\bar{t}$ and QCD-WW background events. A cut on the variable $|\boldsymbol{P}_T^{tot}|$ is correlated with a jet-veto cut, if the jet which triggers the veto originates from the hard-scattering process in which the Higgs boson is produced. However, this variable is largely insensitive to jets which result from pileup effects in the detector. Therefore, a useful rejection can be obtained, even at high LHC luminosity. The only degradation effect expected at high luminosity is a broadening of the $|\boldsymbol{P}_T^{tot}|$ spectrum due to the degraded P_T^{miss} resolution.

– *Central Jet veto:*
Events are rejected if at least one jet with a transverse momentum above 20 GeV/c is found in the pseudorapidity range spanned by the two tag jets. For those channels where $t\bar{t}$ is a significant background, the jet-veto region has been enlarged to cover the pseudorapidity range $-3.2 < \eta < 3.2$. Using this rapidity window, which is usually larger than the gap between the tag jets, events with high jet multiplicities (like $t\bar{t}$ events due to the additional b-jets) are better rejected.

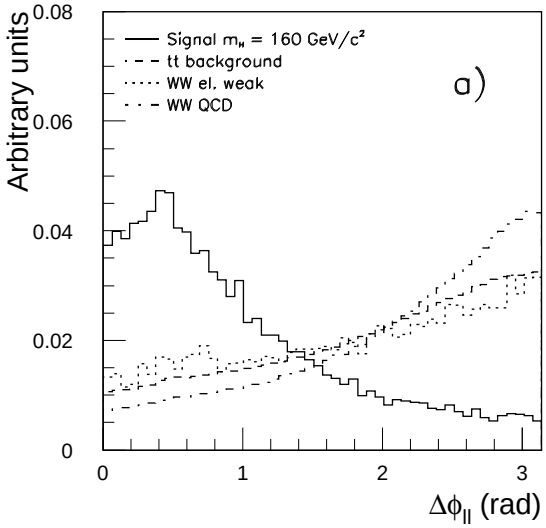

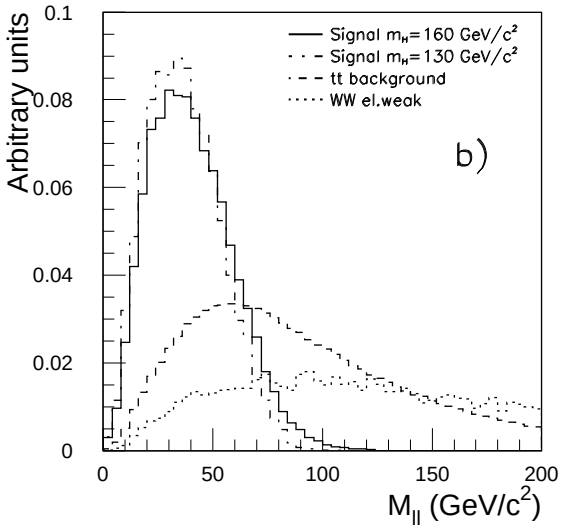

Fig. 3. *a) Azimuthal angle separation $\Delta\phi_{ll}$ between the leptons from signal events with $m_H = 160$ GeV/c^2 and different backgrounds. b) Di-lepton invariant mass distribution for signal events with $m_H = 160$ GeV/c^2 and $m_H = 130$ GeV/c^2, for $t\bar{t}$ and for electroweak WW background. All distributions are normalized to unity.*

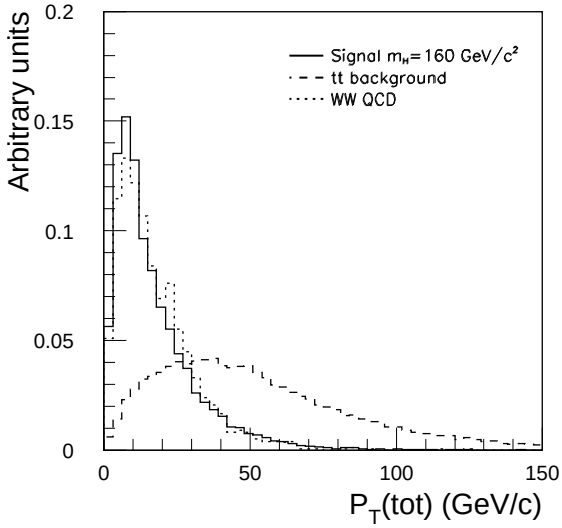

Fig. 4. *Distribution of the momentum balance $|\boldsymbol{P}_T^{tot}|$ between the reconstructed leptons, P_T^{miss} and the tag jets. All distributions are normalized to unity.*

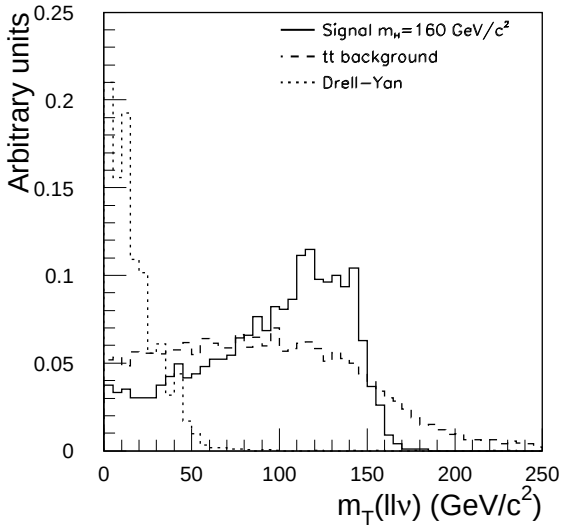

Fig. 5. *Distribution of the transverse mass $m_T(ll\nu)$ of the di-lepton and neutrino system for signal events with $m_H = 160$ GeV/c^2 and for different backgrounds. The distributions are normalized to unity.*

– *Drell-Yan rejection:*
For those processes where same flavour leptons are considered in the final state the Drell-Yan production represents a serious background. This background also exists, although with a lower rate, for e-μ final states via the Drell-Yan production of tau pairs with subsequent double leptonic decays. The $Z \rightarrow ee/\mu\mu$ components can be largely rejected by vetoing those events which have an invariant di-lepton mass compatible with the Z-mass. An efficient rejection of background contributions at low mass can be achieved via cuts on the missing transverse momentum or on the reconstructed transverse mass $m_T(\ell\ell\nu)$ of the di-lepton and neutrino system, which is defined as $m_T(\ell\ell\nu) = \sqrt{2P_T(\ell\ell)P_T^{miss} \cdot (1 - cos\Delta\phi)}$ where $\Delta\phi$ is the angle between the di-lepton vector and the P_T^{miss} vector in the transverse plane. The distributions of this variable for signal, $t\bar{t}$ and Drell-Yan background ($\gamma^*/Z + jets, Z \rightarrow \tau\tau$) are shown in Fig. 5.

– *Tau reconstruction:*
For the $H \rightarrow \tau\tau$ channel, the reconstruction of the τ momenta and thereby the Higgs boson mass is impor-

tant. In the case of the $H \to WW^{(*)}$ decay mode, the tau reconstruction is important for the rejection of the γ^*/Z +jet (with $Z \to \tau\tau$) background.
In signal and background events, the H or Z bosons are emitted with quite high P_T which contributes to large tau boosts and causes the tau decay products to be nearly collinear in the laboratory frame. Within the collinear approximation, *i.e.,* assuming that the tau directions are given by the directions of the visible tau decay products (leptons or hadronic tau respectively), the tau momenta can be reconstructed. Labeling by x_{τ_1} and x_{τ_2} the fraction of the tau energy carried by each lepton or hadronic tau system, the missing transverse momentum vector can be used to solve the two equations for the two unknowns x_{τ_1} and x_{τ_2}. For τ decays, they should lie in the interval $0 < x_{\tau_{1,2}} < 1$. Distributions of the reconstructed variables x_{τ_1} versus x_{τ_2} are shown in Fig. 6 for $H \to \tau\tau$ signal events and background events from electroweak WW production.

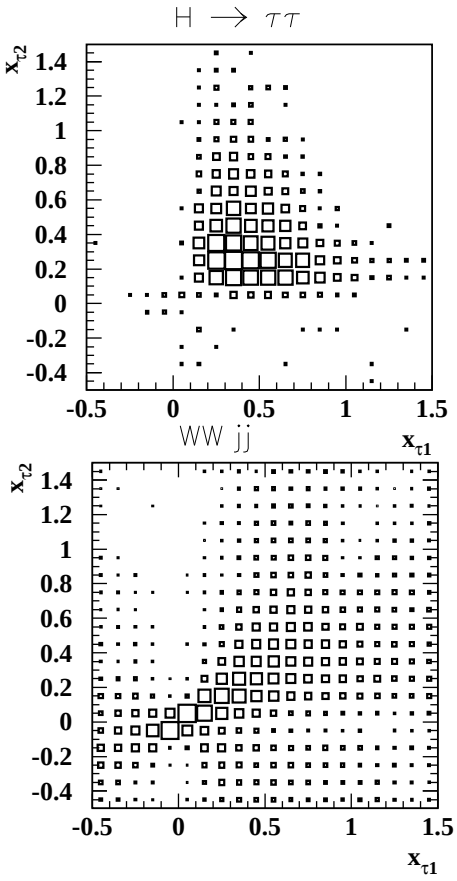

Fig. 6. *Distribution of x_{τ_1} versus x_{τ_2} for $H \to \tau\tau$ signal events with $m_H = 120$ GeV/c^2 (top) and for events from electroweak WW production (bottom).*

– *Mass reconstruction:*
In the case of the $\tau\tau$ decay modes, the Higgs boson mass is given by

$$m_{\tau\tau} = m_{\ell\ell}/\sqrt{x_{\tau_1} x_{\tau_2}}.$$

In the $H \to WW^{(*)}$ decay mode, a direct reconstruction of the Higgs boson mass is not possible, since the longitudinal component of the momentum of the neutrino system can not be reconstructed. For masses below $2m_W$, the (virtual) W bosons are at mostly at rest in the Higgs boson center-of-mass system, resulting in $m_{\ell\ell} \approx m_{\nu\nu}$, so that for both the di-lepton and for the neutrino system the transverse energy can be calculated as [5]

$$E_T^{\ell\ell} = \sqrt{(P_T^{\ell\ell})^2 + m_{\ell\ell}^2},$$

$$E_T^{\nu\nu} = \sqrt{(P_T^{miss})^2 + m_{\ell\ell}^2}.$$

Using these transverse energies the transverse mass of the di-lepton-P_T^{miss} system can be calculated as

$$M_T = \sqrt{(E_T^{\ell\ell} + E_T^{\nu\nu})^2 - (\boldsymbol{p}_T^{\ell\ell} + \boldsymbol{p}_T^{miss})^2}.$$

For Higgs boson masses up to ~ 160 GeV/c^2, this is a good approximation for the Higgs boson transverse mass. Also, above the threshold for the decay into two real W's, the reconstructed mass still contains information about the Higgs boson mass. Again it is found that this definition leads to a sharper signal peak than the previously defined $m_T(\ell\ell\nu)$, where the di-lepton mass has been neglected.

5 The $H \to WW^{(*)}$ decay mode

In this Section the detailed analysis is described for the $H \to WW^{(*)}$ channels. An optimisation of the cuts has been performed in the mass region 160 GeV/c^2< m_H < 180 GeV/c^{2}and for low masses around 120 GeV/c^2. Details can be found in Refs. [20] and [23] respectively.

5.1 Di-lepton final states: $H \to WW^{(*)} \to \ell\nu\ell\nu$

5.1.1 Event selection

In the event selection, the cuts listed in Table 3 have been applied in the two different mass regions. Since it is not expected in the signal that tag jets are b-jets, the selection of tag jet candidates can be enhanced with b-tagging. For instance, in the present analysis $t\bar{t}$ production, which constitutes the largest background, typically has one b-jet identified as a tagging jet. In order to suppress this background it is required that a tag jet candidate is not tagged as b-jet. This requirement can, however, only be applied for the tag jet candidates that fall in the acceptance region of the ATLAS Inner Detector, *i.e.*, $|\eta| < 2.5$. The b-jet efficiency versus rejection against non b-jets has been optimized. A maximum in signal significance has been found for a b-jet efficiency of 0.70 and a corresponding mistag probability of 0.25 for c-quark jets and 0.04 for light quark and gluon jets.

cut	high mass 135 GeV/c^2 $< m_H <$ 190 GeV/c^2	low mass 110 GeV/c^2 $< m_H <$ 135 GeV/c^2
Two leptons with	$P_T^1 > 20$ GeV/c $P_T^2 > 15$ GeV/c $\|\eta\| < 2.5$	$P_T^1(e) > 15$ GeV/c $P_T^1(\mu) > 10$ GeV/c $P_T^2(e) > 15$ GeV/c $P_T^2(\mu) > 10$ GeV/c $\|\eta\| < 2.5$
Tag jets Leptons between tag jets	$P_T^1 > 40$ GeV/c, $P_T^2 > 20$GeV/c $\Delta\eta_{tags} = \|\eta_{tag}^1 - \eta_{tag}^2\| > 3.8$ $\eta_{tag}^{min} < \eta_{l_{1,2}} < \eta_{tag}^{max}$	
Lepton Cuts	$\Delta\phi_{\ell\ell} \leq 1.05$ $\Delta R_{\ell\ell} \leq 1.8$ $\cos\theta_{\ell\ell} \geq 0.2$ $M_{\ell\ell} < 85$ GeV/c^2 $P_T(\ell_{1,2}) < 120$ GeV/c	$\Delta\phi_{\ell\ell} \leq 1.5$ $\Delta R_{\ell\ell} \leq 1.6$ $M_{\ell\ell} < 65$ GeV/c^2
Tau veto	reject events if $x_{\tau_1}, x_{\tau_2} > 0$ $\|M_{\tau\tau} - M_Z\| < 25$ GeV/c^2	
Invariant mass of the two tag jets	$M_{jj} > 550$ GeV/c^2	600 GeV/c^2 $< M_{jj} <$ 2500 GeV/c^2
Transverse momentum balance	$\|\boldsymbol{P}_T^{tot}\| < 30$ GeV/c	
Jet veto	no jets with $P_T > 20$ GeV/c in $\|\eta\| < 3.2$	
$\gamma^*/Z, Z \to \tau\tau$ rejection:	$m_T(\ell\ell\nu) > 30$ GeV/c^2	$m_T(\ell\ell\nu) > 20$ GeV/c^2

Table 3. *Cuts applied in the $H \to WW^{(*)}$ analyses at high and low masses.*

The additional background contributions for the signal from same-flavour leptons, of which the ee and $\mu\mu$ Drell-Yan backgrounds are the dominant ones, can be efficiently rejected by tightening the di-lepton mass cut and by introducing a P_T^{miss} cut:

- $M_{\ell\ell} < 75$ GeV/c^2 and
- $P_T^{miss} > 30$ GeV/c

The acceptance for a Higgs boson with a mass of 160 GeV/c^2 and for the backgrounds after the application of successive cuts is summarized for the $e\mu$ final state in detail in Table 4. Also the contributions to the signal from other Higgs boson production processes have been considered. A significant contribution has been found to arise from the dominant gluon-gluon fusion process $gg \to H \to WW^{(*)}$ where the two tag jets are produced from initial- and final-state radiation. Contributions from the associated production processes WH, ZH or $t\bar{t}H$, where leptons come either from the Higgs boson decays via $WW^{(*)}$ or from the decays of the accompanying vector boson or top-quarks, have been found to be small, with a final accepted cross-section below 0.05 fb and have been neglected.

At the level of the basic acceptance cuts, *i.e.* requiring two leptons and two tag jets with a pseudorapidity separation of $\Delta\eta = 3.8$, the $t\bar{t}$ and the $\gamma^*/Z + jet$ background are each about one order of magnitude larger than the signal. Due to the requirement of forward tag jets, the signal is already at that level dominated by contributions from the vector boson fusion subprocess. The lepton cuts suppress all backgrounds by nearly an order of magnitude, whereas the signal is kept with an efficiency of about 65%. Due to the tau reconstruction, a significant fraction of the electroweak and the $\gamma^*/Z + jet$ background can be rejected, whereas the acceptance for all other processes is high. The cuts on the invariant mass of the tag jets and on the momentum balance significantly suppress all QCD processes, in particular the dominant $t\bar{t}$ background. The signal-to-background ratio can be further improved by applying the central jet veto (mainly $t\bar{t}$ rejection) and the cut on the transverse mass $m_T(ll\nu)$ (rejects mainly the γ^*/Z background). After all cuts, the dominant backgrounds are $t\bar{t}$ and Wt, due to their large production cross-sections, and electroweak WW production, due to its similarity to the signal. For the top backgrounds, the $t\bar{t}$ contribution is larger than the Wt contribution. Out of the 0.66 fb quoted for the sum of the top backgrounds in the upper part of the Table, 0.51 fb are due to $t\bar{t}$ production and 0.15 fb result from single-top production.

All numbers given in the upper part of Table 4 come from direct decays with an electron and a muon in the final state. Di-leptons can, however, also be produced via cascade decays of tau leptons, for example, $W \to \tau\nu \to \ell\nu\bar{\nu}\,\nu$. These contributions have also been calculated and have been added to the accepted signal and background cross-sections. An increase of about 15% for the accepted cross-sections has been found. Due to the softer P_T spectra

	signal (fb)		background (fb)					
	VV	gg	$t\bar{t} + Wt$	$WW + jets$		$\gamma^*/Z + jets$		total
				EW	QCD	EW	QCD	
Lepton acceptance	29.6	121.9	6073	14.2	590.5	5.96	25222	31906
+ Forward Tagging	11.4	2.24	127.5	8.01	1.41	1.55	208.3	346.8
+ Lepton cuts	6.95	1.36	17.0	0.54	0.17	0.50	30.0	48.2
+ τ rejection	6.64	1.34	16.3	0.50	0.17	0.09	5.93	23.0
+ Jet mass	5.30	0.76	10.0	0.50	0.06	0.09	4.01	14.6
+ P_T^{tot}	4.52	0.50	2.34	0.38	0.04	0.07	2.70	5.53
+ Jet veto	3.87	0.34	0.72	0.34	0.03	0.07	1.70	2.86
+ $m_T(\ell\ell\nu)$ cut	3.76	0.31	0.66	0.32	0.02	0.01	0.03	1.04
$H \to WW^{(*)} \to e\mu + X$ incl. $\tau \to e, \mu$ contr.	4.32	0.33	0.75	0.35	0.03	0.01	0.03	1.17
$H \to WW^{(*)} \to ee/\mu\mu + X$ incl. $\tau \to e, \mu$ contr.	3.92	0.30	0.71	0.36	0.04	0.04	0.12	1.27

Table 4. *Accepted signal (for $m_H = 160$ GeV/c^2) and background cross-sections in fb for the $H \to WW \to e\mu\nu\nu$ channel after the application of successive cuts. For the signal, the contributions via the vector boson fusion (VV) and the gluon fusion channel (gg) are given separately. The last two lines give the final numbers if the contributions from $W \to \tau\nu \to l\nu\nu\ \nu$ are added for both the $e\mu$ and the $ee/\mu\mu$ final states.*

of leptons from tau decays this contribution is smaller than expected from a scaling of branching ratios.

The final acceptance including the contributions from τ cascade decays, is also given for the sum of the ee and $\mu\mu$ final states. Due to the additional cuts the signal acceptance is lower than in the $e\mu$ case. However, the P_T^{miss} and the $M_{\ell\ell}$ cuts are very efficient in rejecting the additional $\gamma^*/Z + jet$ background, such that also in this channel, a convincing Higgs boson signal for Higgs boson masses around 160 GeV/c^2 can be expected.

After all cuts, a signal in the $e\mu$ channel for a Higgs boson with a mass of 160 GeV/c^2 of the order of 4.6 fb is found above a total background of 1.2 fb. Due to this large signal-to-background ratio, this channel alone has a good discovery potential for a Higgs boson with a mass around 160 GeV/c^2 and is not very sensitive to systematic uncertainties on the level of the background. This compares favourably with the $gg \to WW^{(*)}$ channel previously studied [1,24]. For an integrated luminosity of 30 fb^{-1} and for a Higgs boson mass of 160 GeV/c^2, the background for the inclusive channel was found to be at a level of 650 events with a signal-to-background ratio of 0.60.

The corresponding numbers for a Higgs boson with a mass of 120 GeV/c^2 are given in Table 5. Due to the suppressed branching ratio, the signal significance is reduced for lower Higgs boson masses. The contributions from cascade decays via tau leptons are found to be larger than in the high mass case, due to the lower P_T-thresholds used for the leptons. These contributions are included in the numbers given in Table 5.

In the present study, numbers for signal and background have been found which are somewhat different from the numbers quoted in the original parton-level study of Ref. [5]. A detailed comparison between both simulations has been performed. If identical cuts as in Ref. [5] are applied, the lepton acceptance is found to be about 20% lower. In addition, the efficiency for reconstructing the tag jets has been found to be lower by 15%. It has been traced back that both losses are related to initial- and final-state gluon radiation. They lead to a degraded lepton isolation as well as to non-Gaussian tails in the jet response which can not be fully corrected in jet calibration procedures. However, the main conclusion of Ref. [5], that the search for vector boson fusion in the intermediate mass range at the LHC has a large discovery potential for a Standard Model Higgs boson in the $H \to WW^{(*)}$ decay channel, is confirmed by the present studies based on a more realistic detector simulation.

5.1.2 Uncertainties on the background

All QCD-type backgrounds quoted in the previous section have been calculated using the PYTHIA parton-shower Monte Carlo. Due to the requirement of two hard tag jets in the final state, the final number of predicted background events is sensitive to the hard tail of the jet distribution in $t\bar{t} + jet$ or $WW + jet$ events.

	signal (fb)		background (fb)					
	VV	gg	$t\bar{t} + Wt$	$WW + jets$		$\gamma^*/Z + jets$		total
				EW	QCD	EW	QCD	
Lepton acceptance	5.20	17.30	8456	17.1	617.2	7.09	4980	14077
+ Forward Tagging	1.85	0.27	82.6	10.7	1.83	2.10	45.2	142.4
+ Lepton angular cuts	1.36	0.18	13.5	0.89	0.27	0.81	7.47	22.9
+ τ rejection	1.27	0.18	12.9	0.83	0.27	0.15	1.64	15.8
+ Jet mass	0.88	0.08	6.39	0.43	0.08	0.11	0.83	7.84
+ P_T^{tot}	0.68	0.05	1.40	0.32	0.04	0.10	0.46	2.32
+ Jet veto	0.59	0.05	0.61	0.28	0.04	0.10	0.32	1.35
+ $m_T(\ell\ell\nu)$-cut	0.52	0.05	0.58	0.27	0.03	0.02	0.05	0.95
$H \to WW^{(*)} \to e\mu + X$	0.52	0.05	0.58	0.27	0.03	0.02	0.05	0.95
$H \to WW^{(*)} \to ee/\mu\mu + X$	0.50	0.04	0.58	0.30	0.03	0.03	0.39	1.33

Table 5. *Accepted signal (for $m_H = 120$ GeV/c^2) and background cross-sections in fb for the $H \to WW \to e\mu\nu\nu$ channel after the application of successive cuts (upper part). The final numbers for both $e\mu$ and $ee/\mu\mu$ final states are given in the last two lines. The contributions from $W \to \tau\nu \to \ell\nu\nu\ \nu$ are included in all numbers quoted.*

In order to get an estimate on the systematic uncertainties on the background predictions, the dominant $t\bar{t}+jet$ background has also been evaluated using explicit matrix element calculations for $t\bar{t} + 0\ jet$, $t\bar{t} + 1\ jet$ and $t\bar{t} + 2\ jet$ final states. These matrix element calculations have been provided by the authors of Ref. [5] and have been interfaced to the PYTHIA generator. In order to avoid double counting when adding the three contributions, the procedure proposed in Ref. [5], to define three distinct final-state jet topologies, has been adopted. For $t\bar{t}$ $+0\ jets$ only the two b-jets are considered as tag jet candidates. Initial- and final-state radiation in these events may lead to a rejection of the event due to the jet veto. A distinctively different class is defined by those $t\bar{t}\ + 1\ jet$ events where the final-state light quark or gluon gives rise to one tag jet and one of the two b-jets is identified as the other tag jet. Finally, a third class is defined where in $t\bar{t}\ + 2\ jets$ the final-state light quarks or gluons are identified as tag jets.

The three final-state topologies have been simulated separately in PYTHIA. In the generation, a parton-level P_T cutoff of 10 GeV/c has been introduced to regulate the divergencies appearing in the tree-level matrix elements. If the cross-section contributions of the three processes are added, the total $t\bar{t}$ background is estimated to be 1.08 fb, which is a factor of 2.1 higher than the value determined with the PYTHIA parton-shower approach [20]. This simple addition may overestimate the true $t\bar{t}$ background since the divergencies in the tree-level calculations are not compensated for by P_T dependent topological K-factors, which may take values smaller than 1 in the low-P_T region. Therefore, this estimate is used in the evaluation of the signal significance as a conservative estimate of the $t\bar{t}\ + jet$ background. The distribution of the transverse mass M_T, assuming this background estimate, is shown in Fig. 7 for Higgs boson signals of 160 GeV/c^2 and 120 GeV/c^2.

Given the major uncertainties in predicting the absolute level of the $t\bar{t}$ background, it is important to determine this background directly in the experiment. As mentioned already above, only a transverse mass peak can be reconstructed. After all cuts are applied, most background events lie in the same region of transverse mass as the signal. It is expected that at least the shape of the dominant $t\bar{t}$ background can be determined from $t\bar{t}$ events observed at the LHC. In $t\bar{t}$ events one may require only one leptonic decay and reconstruct the second top decaying into three jets. After requiring the forward jet tag criteria in addition, and correcting for differences in reconstruction efficiencies, this should provide an absolute prediction of the background rate with small uncertainties.

In addition, the selection cuts can be varied. An interesting approach is, for example, to apply all cuts discussed above except the lepton cuts, as defined in Table 3. The distribution of the reconstructed transverse mass M_T is shown for a Higgs boson signal with $m_H = 160$ GeV/c^2 above the backgrounds in Fig. 8 without applying the lepton cuts. Even if no lepton cuts are applied, a clear signal can be seen above a background which now extends to higher M_T values. The background in the high-M_T region can be used to perform a normalization outside of the signal region and to predict the background below the signal peak, if the shape of the distribution is taken from a Monte Carlo prediction. Already for an integrated luminosity of 10 fb^{-1}, a statistical uncertainty of about 10% for the predicted background can be reached. In addition,

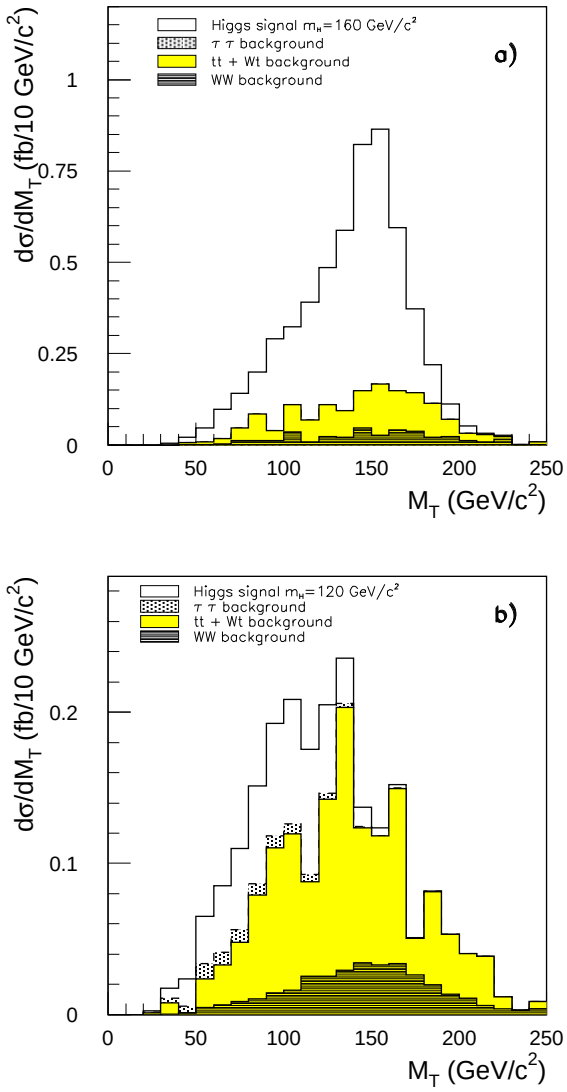

Fig. 7. *Distributions of the transverse mass M_T for Higgs boson masses of (a) 160 GeV/c^2 and (b) 120 GeV/c^2 in the eμ-channel after all cuts are applied. The accepted cross-sections $d\sigma/dM_T$ (in fb/10 GeV/c^2) including all efficiency and acceptance factors are shown in both cases.*

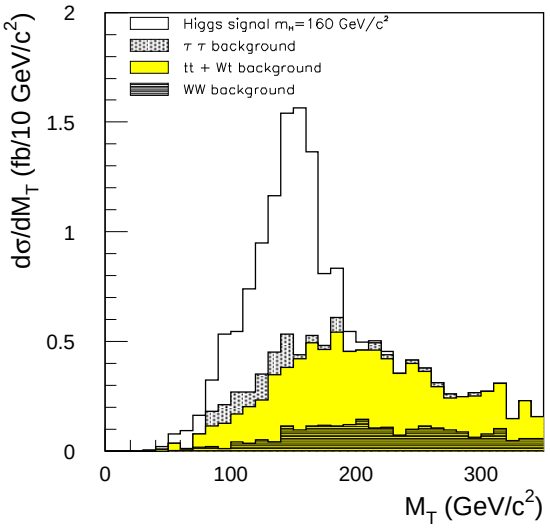

Fig. 8. *Distribution of the transverse mass M_T for a Higgs boson mass of 160 GeV/c^2 in the eμ-channel above the sum of the various backgrounds after all cuts except the lepton cuts (see Table 3) are applied. The accepted cross-section $d\sigma/dM_T$ (in fb/10 GeV/c^2) including all efficiency and acceptance factors is shown.*

as discussed in the following subsection, the distribution of the azimuthal difference $\Delta\phi$ between the two leptons can be used to extract a background normalization for events below the signal peak. Given these additional possibilities, it is conservatively assumed in the following that the total background rate can be determined with an uncertainty of $\pm 10\%$.

5.1.3 Consistency with a spin-0 resonance in $H \to WW^{(*)}$ decays

The relaxed selection criteria can also be used to extract additional information on the spin of the Higgs boson in the $H \to WW^{(*)}$ decay mode. As discussed above, the dilepton azimuthal angular separation $\Delta\phi$ is sensitive to the spin of the Higgs boson. The selection obtained without applying the lepton cuts allows an unbiased $\Delta\phi$ distribution to be reconstructed. In Fig. 9, this distribution is shown for $e\mu$ final states passing all cuts except the lepton cuts. For this example, corresponding to a Higgs boson mass of 160 GeV/c^2, the events have been separated into two different regions of M_T, (a) in the so called signal region ($M_T < 175$ GeV/c^2) and (b) in a control region ($M_T > 175$ GeV/c^2). For events in the signal region, the distribution shows the effect of a spin-0 resonance above a flat background. The pronounced structure at small $\Delta\phi$ is not present for events in the control sample, where the $t\bar{t}$ and WW backgrounds are expected to dominate. Therefore, the unbiased $\Delta\phi$ distribution in the signal region can be used for both a demonstration of the consistency of the signal with a spin-0 hypothesis and for an additional background normalization. This normalization can be performed in the high $\Delta\phi$ region directly from events below the peak.

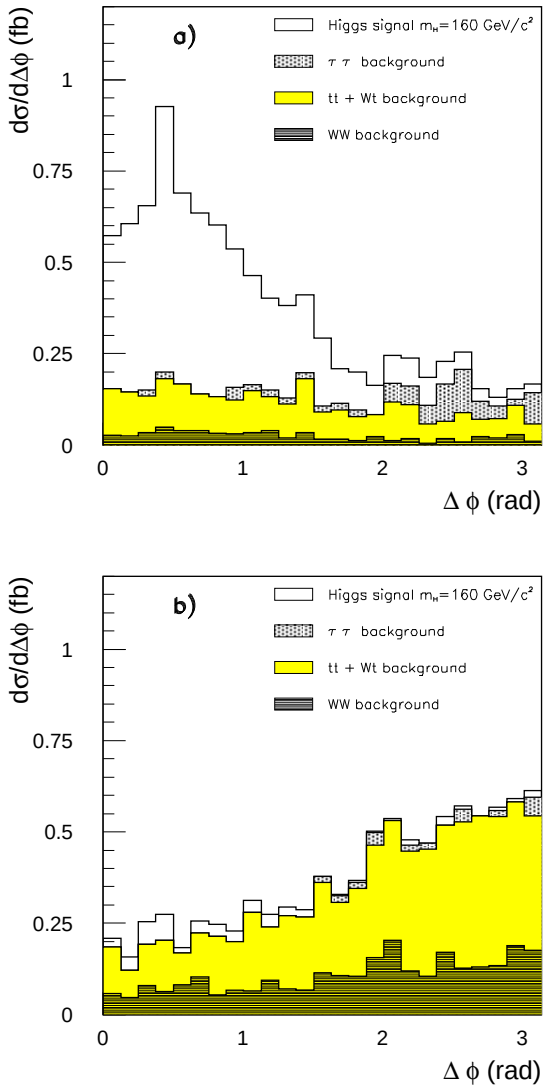

Fig. 9. *Distributions of the azimuthal opening angle $\Delta\phi$ between the two leptons for (a) events in the signal region ($M_T < 175$ GeV/c^2) and (b) events outside the signal region ($M_T > 175$GeV/c^2). The accepted cross-sections $d\sigma/dM_T$ (in fb/10 GeV/c^2) including all efficiency and acceptance factors are shown in both cases.*

5.2 The $\ell\nu$-jet-jet channel

In addition to the di-lepton final states, a study has been made as to whether the larger branching ratio of the W-bosons into quark pairs can be used and the process $qq \rightarrow qqH \rightarrow qqWW^{(*)} \rightarrow qq\ \ell\nu\ jj$ can be identified above the larger backgrounds. This process has already been established as a discovery channel for a heavy Higgs boson [1] in the vector boson fusion process, but has so far not been considered in the intermediate mass region.

Due to the larger hadronic branching ratio of the W into a $q\bar{q}$-pair, the cross-section times branching ratio for this channel is about 4.3 times larger than for the di-lepton channel. However, since there is only one lepton in the final state, $W + jet$ production is a serious additional background, with a cross-section which is more than two orders of magnitude larger than the signal cross-section. The W+4 jet background has been evaluated using both the PYTHIA parton-shower approach and the VECBOS [26] explicit matrix element calculation. The VECBOS prediction has been found to be a factor of two larger. Since VECBOS describes well the measurements of W+jet production at the TeVatron [27,28], it has been used also for the background estimate in this study. In order to suppress this large background, very tight cuts on the tag jets have been applied. The two jets from the W decay are searched for in the central region of the detector, $|\eta| < 2.0$. The invariant mass of the two jets is required to be compatible with the W mass. A mass window cut is applied for Higgs boson searches with $m_H > 160$ GeV/c^2, where two on-shell W's are expected. For lower Higgs boson masses, the lower mass cut has been removed since the jets may also originate from an off-shell W boson. Similar to the di-lepton analysis, angular correlations resulting from the decay of the scalar Higgs boson into two vector bosons are exploited. Detailed studies have shown [25] that in this case, cuts on the minimal and maximal separation between the lepton and the jets from the W decay, $\Delta R_{min} = min(\Delta R(l, j_1), \Delta R(l, j_2))$ and $\Delta R_{max} = max(\Delta R(l, j_1), \Delta R(l, j_2))$, lead to an improved signal-to-background ratio.

The cuts applied in this analysis are:

- One isolated lepton with
  30 GeV/c $< P_T <$ 100 GeV/c and $|\eta| < 2.5$ and
  missing transverse momentum $P_T^{miss} > 30$ GeV/c.
- Two tag jets with $P_T > 60$ GeV/c,
  $\Delta\eta_{tags} = |\eta^1_{tag} - \eta^2_{tag}| > 5.0$ and
  $M_{jj} > 1200$ GeV/c^2.
  In addition, the number of jets with $P_T > 20$ GeV/c in the forward region of the detector ($2 < |\eta| < 5$) is required to be smaller than 5.
- Cuts on jets in the central region: two jets in the central region ($|\eta| < 2.0$) with:
  30 GeV/c $< P_T(j_1) <$ 100 GeV/c and
  25 GeV/c $< P_T(j_2) <$ 75 GeV/c and
  65 GeV/c$^2 < M(j_1, j_2) <$ 90 GeV/c^2 for $m_H \geq 160$ GeV/c^2 and
  $M(j_1, j_2) <$ 90 GeV/c^2 for $m_H <$ 160 GeV/c^2.
- Jet veto: no additional jets with $P_T > 20$ GeV/c in the central region $|\eta| < 2.0$.
- Angular cuts: $\Delta R_{min} < 1$ and $\Delta R_{max} < 2$ for $m_H \geq 160$ GeV/c^2 and
  $\Delta R_{min} < 0.8$ and $\Delta R_{max} < 1.4$ for $m_H <$ 160 GeV/c^2.

	signal	background (fb)				
	VV (fb)	$t\bar{t}$	W+jet	$WW + jets$		Total
				EW	QCD	
Lepton acceptance + P_T^{miss}	40.5	3300	20000	22.3	65.3	23388
+ Tag jets, incl. mass cut	5.8	135	690	11.6	0.1	837
+ Central Jets	1.6	9.0	14.9	2.5	<0.01	26.4
+ Jet veto	1.5	2.4	7.7	2.2	<0.01	12.3
+ Angular Cuts	0.8	0.1	0.4	0.1	<0.01	0.6

Table 6. *Accepted signal (for $m_H = 160$ GeV/c^2) and background cross-sections in fb for the $H \to WW \to l\nu jj$ channel after the application of successive cuts.*

The acceptance of the cuts for a Higgs boson signal of 160 GeV/c^2 and for the backgrounds is summarized in Table 6.

As can be seen from these numbers, the final signal rates after all cuts are expected to be much lower than the corresponding numbers in the di-lepton channel, with a much smaller signal-to-background ratio. A possible observation of a Higgs boson with a mass around 160 GeV/c^2 can be confirmed in this channel for integrated luminosities around 30 fb^{-1}. However, there might be large systematic uncertainties on the estimate of the dominant W+jet background. In addition, it must be stressed that very hard cuts on the P_T and on the invariant mass of the forward tag jets, as well as on the separation ΔR between the lepton and the jets from the W-decay, are necessary to extract the signal above the large backgrounds. These extreme cuts might also lead to larger systematic uncertainties on the background prediction.

5.3 Discovery potential as a function of mass

The analyses outlined above has been performed in the full range of Higgs boson masses from 110 to 190 GeV/c^2. As illustrated in Fig. 7, Higgs boson signal events are mainly reconstructed in the region of transverse mass 50 GeV/c^2,$< m_T < m_H + 10$ GeV/c^2. For Higgs boson masses above the threshold of two real W bosons ($m_H > 160$ GeV/c^2) the upper mass bound has to be increased to optimize the signal significance. The upper mass bounds are given in Table 7 together with the expected numbers of signal and background events in the corresponding interval of transverse mass for all three $WW^{(*)}$ channels considered for an integrated luminosity of 10 fb^{-1} (respectively 30 fb^{-1} for the $\ell\nu$ *jet jet*-channel).

A signal-to-background ratio larger than 1 is found in the di-lepton channels for $m_H > 130$ GeV/c^2. The signal significance, expressed in the equivalent number of Gaussian standard deviations, has been calculated assuming an integrated luminosity of 10 fb^{-1}, the conservative estimate of the $t\bar{t}$ background and a systematic uncertainty of 10% on the level of the background below the signal peak. Since the numbers of signal and background events are small, Poisson statistics has been used in the evaluation of the signal significance. With 10 fb^{-1}, a 5σ discovery can be claimed for $145 < m_H < 190$ GeV/c^2 in the $e\mu$ channel alone. For an integrated luminosity of 30 fb^{-1} the discovery range increases to $125 < m_H < 190$ GeV/c^2 if both di-lepton channels are combined. Already with an integrated luminosity of 5 fb^{-1} only, a mass interval from 150 - 190 GeV/c^2 can be covered. The conservative assuption of the larger $t\bar{t}$ background only slightly affects the discovery potential. In Fig. 10, the signal significance is shown as a function of the Higgs boson mass for both assumptions of the $t\bar{t}$ background and for an integrated luminosity of 10 fb^{-1}.

6 The $H \to \tau\tau$ decay mode

In the following, searches for $H \to \tau\tau$ decays using the double leptonic decay mode, $qqH \to qq\,\tau\tau \to qq\,l^+\nu\bar{\nu}\,l^-\bar{\nu}\nu$ and the lepton-hadron decay mode $qqH \to qq\ \tau\tau \to qq\ l^{\pm}\nu\nu\ had\ \nu$, are described. The analysis strategy follows to a large extent the one described above for the WW decay modes. The same backgrounds as considered in the WW analysis are also relevant here. The $Z + jet$ production, followed by the $Z \to \tau\tau$ decay, constitues the principal background for $H \to \tau\tau$ decays at low Higgs boson masses. This background has been evaluated using a matrix element based Monte Carlo generator. The main points of the analyses are briefly summarized in the following subsections. For details the reader is referred to Refs. [14], [29], [30] and [31].

6.1 Di-lepton final states: $H \to \tau\tau \to \ell^+\ell^- P_T^{miss} + X$

The following cuts have been applied to select the various di-lepton final states:

– Two isolated leptons with
$P_T(e) > 15$ GeV/c and $|\eta_e| \leq 2.5$ and

m_H ($\mathrm{GeV/c^2}$)	110	120	130	140	150	160	170	180	190
Upper M_T bound for mass window ($\mathrm{GeV/c^2}$)	120	130	140	150	160	175	190	220	240
$H \to WW^{(*)} \to e\mu + X$									
Signal ($10\ \mathrm{fb}^{-1}$)	1.4	4.9	12.3	16.3	26.2	42.5	42.7	35.6	27.8
Background ($10\ \mathrm{fb}^{-1}$)	5.8	7.1	9.2	8.1	9.8	12.4	13.8	16.3	17.1
Stat. significance ($10\ \mathrm{fb}^{-1}$)	0.5	1.5	3.2	4.2	6.0	8.1	7.8	6.3	5.0
$H \to WW^{(*)} \to ee/\mu\mu + X$									
Signal ($10\ \mathrm{fb}^{-1}$)	1.3	4.6	11.7	16.4	27.8	40.2	44.8	36.0	25.9
Background ($10\ \mathrm{fb}^{-1}$)	6.7	8.7	10.1	10.0	12.2	14.3	15.9	18.4	19.2
Stat. significance ($10\ \mathrm{fb}^{-1}$)	0.4	1.3	2.9	3.9	5.8	7.4	7.7	6.1	4.5
$H \to WW^{(*)} \to l\nu\ jj$									
Signal ($30\ \mathrm{fb}^{-1}$)	-	-	4.5	7.5	10.5	24.0	24.0	18.0	15.0
Background ($30\ \mathrm{fb}^{-1}$)	-	-	6.0	6.0	6.0	18.0	18.0	18.0	18.0
Stat. significance ($30\ \mathrm{fb}^{-1}$)	-	-	1.5	2.4	3.3	4.6	4.6	3.5	3.0
Combined Stat. significance ($10\ \mathrm{fb}^{-1}$)	0.8	2.1	4.4	5.9	8.4	11.0	11.0	8.8	6.8

Table 7. *Expected signal and background rates and signal significance for the three $WW^{(*)}$ decay channels as a function of m_H assuming an integrated luminosity of 10 fb^{-1} (30 fb^{-1} for the $H \to WW^{(*)} \to l\nu\ jj$ channel). The signal significance has been computed using Poisson statistics and assuming a systematic uncertainty of 10% on the background. The conservative estimate for the $t\bar{t}$ background has been used.*

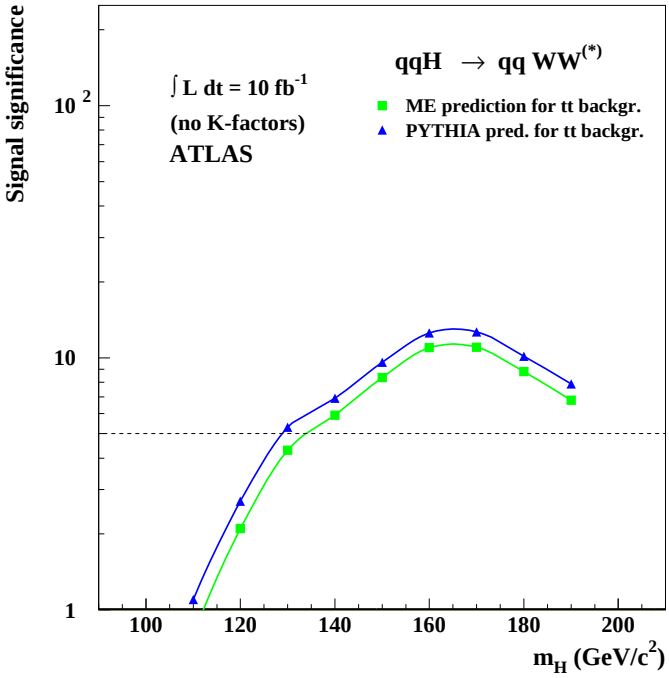

Fig. 10. *ATLAS sensitivity for the discovery of a Standard Model Higgs boson in the $qqH \to qqWW$ channel for an integrated luminosity of 10 fb^{-1} . The signal significance is plotted for the combination of the three channels considered and for two estimates of the $t\bar{t}$ background. This background has been computed using the PYTHIA parton-shower approach as well as the explicit matrix element calculation for $t\bar{t} + 0, 1,$ and 2 jets.*

$P_T(\mu) > 10$ GeV/c and $|\eta_\mu| \leq 2.5$.
In addition, a b-jet veto is applied, *i.e.*, the event is rejected if a b-jet with $P_T > 20$ GeV/c and $|\eta| < 2.5$ is identified. A b-jet tagging efficiency of 0.6 is assumed [1].
- Two tag jets with $P_T^1 > 50$ GeV/c, $P_T^2 > 30$ GeV/c and $\Delta\eta_{tags} = |\eta_{tag}^1 - \eta_{tag}^2| \geq 4.4$.
  In addition, it has been required that the leptons be reconstructed within the pseudorapidity gap spanned by the two tag jets: $\eta_{tag}^{min} < \eta_{l_{1,2}} < \eta_{tag}^{max}$.
- Missing transverse momentum:
  $P_T^{miss} > 50$ GeV/c.
- Invariant mass of the two tag jets:
  $M_{jj} > 700$ GeV/c^2.
- Jet veto: no jets with $P_T > 20$ GeV/c in $|\eta| < 3.2$.
- Azimuthal separation $\Delta\phi_{jj}$ between the tag jets: $\Delta\phi_{jj} < 2.2$.
  This cut is applied to reduce the electroweak Zjj background, for which back-to-back jets are preferred [32].
- Separation between the two leptons: $\Delta R_{\ell\ell} < 2.6$.
- Tau reconstruction:
  $x_{\tau_1}, x_{\tau_2} > 0, \qquad x_{\tau_1}^2 + x_{\tau_2}^2 < 1.$
- Mass window around the Higgs boson mass:
  $m_H - 10$ GeV/c$^2 < m_{\tau\tau} < m_H + 15$ GeV/c^2.

The results of the analysis are summarized in Table 8. The accepted cross-sections for the signal with $m_H = 120$ GeV/c^2 and the background contributions are given after the application of the consecutive cuts for the $e\mu$ channel. The final numbers are also included for ee and $\mu\mu$ final states.

A similar rejection pattern as seen in the $H \to WW^{(*)}$ analysis can be observed. It should be pointed out that the tau reconstruction with cuts on x_{τ_1} and x_{τ_2} leads to a significant suppression of the reducible backgrounds, while the signal is kept with high efficiency. After τ reconstruction the signal-to-background ratio is still much smaller than 1. This situation is drastically changed after the application of the mass cut around the Higgs boson mass. The sidebands can be used for the determination of the absolute level of the background. The mass window and therefore the background level depend on the $\tau\tau$ mass resolution. This resolution has so far only be determined with the ATLAS fast detector simulation, where a value of 12 GeV/c^2 has been found for a Higgs boson with a mass of 120 GeV/c^2. A verification of this mass resolution in a full detector simulation remains to be done. However, based on the experience gained in the MSSM decay channels $A/H \to \tau\tau$ [19], no big differences between fast and full simulations are expected.

For a Higgs boson with a mass of 120 GeV/c^2, the dominant background results from $Z+jet$ production. Despite the good signal-to-background ratio found, the accepted cross-sections are low and a data sample corresponding to 20-30 fb^{-1} is needed for a significant observation of a Higgs boson in this channel. Therefore, an observation of the $H \to \tau\tau$ decay mode at the LHC in the vector boson fusion process looks feasible, as suggested in Ref. [6].

All numbers given in the upper part of Table 8 refer to $e\mu$ final states. The final numbers, after the application of all cuts, for the ee and $\mu\mu$ final states are given in the last two lines of the table. The contributions from other sources of Higgs boson production have also been evaluated. The contribution from the gluon fusion is found to be small, and contributes after all cuts at a level of about 4% of the vector boson fusion cross-section to the Higgs boson signal. Also the contributions via $H \to WW^{(*)} \to \ell\ell P_T^{miss}$ to the signal have been evaluated. Due to the strong variation of the $WW^{(*)}$ branching ratio with the Higgs boson mass, this contribution is found to be mass dependent. It ranges between 0.003 fb for $m_H = 110$ GeV/c^2 and 0.03 fb for $m_H = 150$ GeV/c^2. Since for those events the reconstructed $\tau\tau$ mass does not correspond to the Higgs boson mass, these contributions have been added to the background in the evaluation of teh signal significance.

The distribution of the reconstructed $\tau\tau$ invariant mass for the $e\mu$ final state is shown in Fig. 11 for a Higgs boson signal of 120 GeV/c^2 above the background for an integrated luminosity of 30 fb^{-1}.

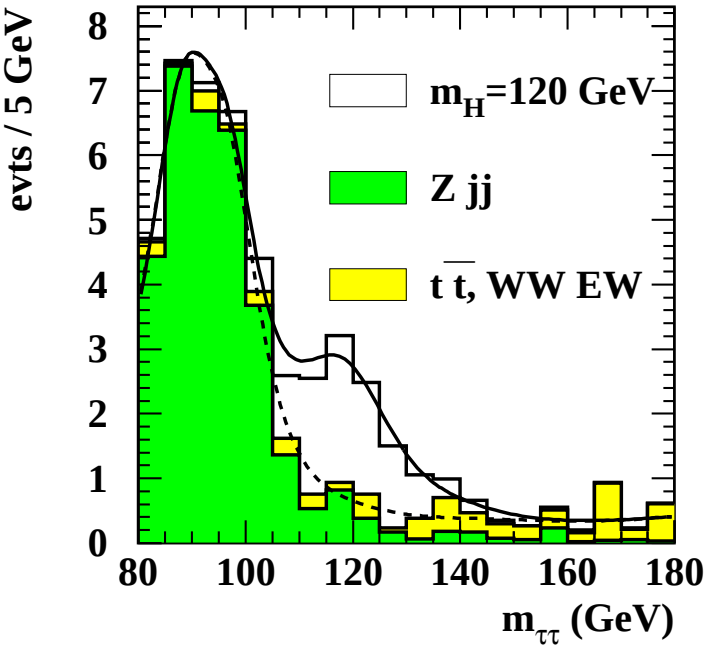

Fig. 11. *The reconstructed $\tau\tau$ invariant mass for a Higgs boson signal of 120 GeV/c^2 in the $e\mu$ channel above all backgrounds after application of all cuts except the mass window cut. The number of signal and background events are shown for an integrated luminosity of 30 fb^{-1}.*

	signal (fb)		background (fb)					
	VV	gg	$t\bar{t}+jets$	$WW+jets$		$\gamma^*/Z+jets$		Total
				EW	QCD	EW	QCD	
Lepton acceptance	5.55		2014.	18.2	669.8	11.6	2150.	4864.
+ Forward Tagging	1.31		42.0	9.50	0.38	2.20	27.5	81.6
+ P_T^{miss}	0.85		29.2	7.38	0.21	1.21	12.4	50.4
+ Jet mass	0.76		20.9	7.36	0.11	1.17	9.38	38.9
+ Jet veto	0.55		2.70	5.74	0.05	1.11	4.56	14.2
+ Angular cuts	0.40		0.74	1.20	0.04	0.57	3.39	5.94
+ Tau reconstruction	0.37		0.12	0.28	0.001	0.49	2.84	3.73
+ Mass window	0.27	0.01	0.03	0.02	0.0	0.04	0.15	0.24
$H \to \tau\tau \to e\mu$	0.27	0.01	0.03	0.02	0.0	0.04	0.15	0.24
$H \to \tau\tau \to ee$	0.13	0.01	0.01	0.01	0.0	0.02	0.07	0.11
$H \to \tau\tau \to \mu\mu$	0.14	0.01	0.01	0.01	0.0	0.02	0.07	0.11

Table 8. *Accepted signal (for $m_H = 120$ GeV/c^2) and background cross-sections in fb for the $H \to \tau\tau \to e\mu + X$ channel after the application of successive cuts. For the signal, the contributions via the vector boson fusion and the gluon fusion channel are given separately. The final results for ee and $\mu\mu$ final states are given in the last rows of the table.*

6.2 The lepton-hadron decay mode: $H \to \tau\tau \to \ell\nu\nu\ had\ \nu$

The lepton-hadron final states are selected by applying the following cuts:

- One isolated lepton (e or μ) with
  $P_T(e) > 25$ GeV/c and $|\eta_e| \leq 2.5$ or
  $P_T(\mu) > 20$ GeV/c and $|\eta_\mu| \leq 2.5$.
- One identified hadronic τ cluster in the calorimeter with $P_T > 40$ GeV/c passing the standard ATLAS tau selection criteria [1,19]. In the present analysis, a selection with an efficiency of 50% for hadronic tau decays has been used.
- Two tag jets with $P_T^1 > 40$ GeV/c, $P_T^2 > 20$ GeV/c and $\Delta\eta_{tags} = |\eta_{tag}^1 - \eta_{tag}^2| \geq 4.4$.
  In addition, it has been required that the visible tau decay products be reconstructed within the pseudorapidity gap spanned by the two tagging jets: $\eta_{tag}^{min} < \eta_{\ell,h} < \eta_{tag}^{max}$.
- Tau reconstruction:
  $0 < x_{\tau_\ell} < 0.75$ and $0 < x_{\tau_h} < 1$,
  where x_{τ_ℓ} and x_{τ_h} are the corresponding momentum fractions carried by the lepton or the hadronic tau system respectively.
- Transverse mass cut: in order to suppress the $t\bar{t}$ background, where the lepton and the missing transverse momentum originate from the decay of a W, a cut on the transverse mass
  $m_T(\ell\nu) = \sqrt{2P_T(\ell)P_T^{miss} \cdot (1 - cos\Delta\phi)}$ is applied:
  $m_T(\ell\nu) < 30$ GeV/c^2.
- Missing transverse momentum:
  $P_T^{miss} > 30$ GeV/c.
- Invariant mass of the two tag jets:
  $M_{jj} > 700$ GeV/c^2.
- Jet veto: no jets with $P_T > 20$ GeV/c in the pseudorapidity range defined by the two tag jets $\eta_{tag}^{min} < \eta_j^{veto} < \eta_{tag}^{max}$.
- Mass window around the Higgs boson mass:
  $m_H - 10$ GeV/c^2 $< m_{\tau\tau} < m_H + 15$ GeV/c^2.

The results of the analysis are summarized in Table 9, where the accepted cross-sections for the signal with $m_H = 120$ GeV/c^2 and the background contributions are given after the application of the consecutive cuts.

A similar rejection pattern as for the di-lepton decay mode can be observed. Also in this channel, the $Z + jet$ production constitutes the largest background and a signal-to-background ratio larger than 1 can only be achieved after the final mass window cut has been applied. Also for this channel the mass resolution has been determined with the ATLAS fast detector simulation and has been found to be 11 GeV/c^2 for a Higgs boson with a mass of 120 GeV/c^2.

The distribution of the reconstructed $\tau\tau$ invariant mass for the $\ell - had$ final state is shown in Fig. 12 for a Higgs boson mass of 130 GeV/c^2 above the background for an integrated luminosity of 30 fb^{-1}.

6.3 Systematic uncertainties for the $H \to \tau\tau$ channels

Since a $\tau\tau$ mass peak can be reconstructed, the absolute level of the background can be estimated from sidebands in the distribution. This is assumed to work well in the mass region $m_H > 125$ GeV/c^2, since there the Higgs mass

	signal (fb)		background (fb)				
	VV	gg	$t\bar{t}$	$\gamma^*/Z + jets$ QCD	$\gamma^*/Z + jets$ EW	W+jet	Total
Lepton acceptance	13.7	50.3	$1.6{\cdot}10^4$	6925	22.0	$3.4{\cdot}10^4$	$5.7{\cdot}10^4$
+ Identified had. τ	6.18	22.7	4274.	1842	8.03	3200.	9462
+ Forward Tagging	1.97	0.18	29.7	23.6	1.72	30.0	85.0
+ Tau reconstruction	1.27	0.11	6.06	13.8	1.09	5.9	26.9
+ Transverse mass	1.02	0.07	1.74	11.9	0.92	0.63	15.2
+ P_T^{miss}	0.81	0.05	1.38	8.31	0.71	0.58	11.0
+ Jet mass	0.71	0.03	1.01	6.63	0.69	0.37	8.70
+ Jet veto	0.63	0.02	0.14	4.24	0.66	0.21	5.25
+ Mass window	0.52	0.01	0.01	0.19	0.06	<0.01	0.27

Table 9. *Accepted signal (for $m_H = 120$ GeV/c^2) and background cross-sections in fb for the $H \to \tau\tau \to \ell\nu\nu$ had ν channel after the application of successive cuts. For the signal, the contributions via the vector boson fusion and the gluon fusion channel are given separately.*

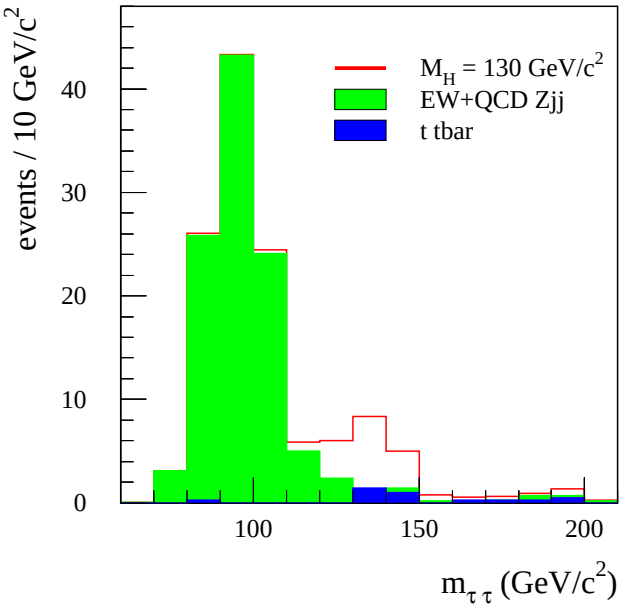

Fig. 12. *The reconstructed $\tau\tau$ invariant mass for a Higgs boson signal of 130 GeV/c^2 in the ℓ – had channel above all backgrounds after application of all cuts except the mass window cut. The number of signal and background events are shown for an integrated luminosity of 30 fb^{-1}.*

peak is well separated from the $Z \to \tau\tau$ background peak. For masses in the range between 110 and 125 GeV/c^2, the level still can be determined from a normalization to the $Z \to \tau\tau$ background peak. However, in this case uncertainties on the shape of the sum of the $Z \to \tau\tau$ resonance and the remaining $t\bar{t}$ background are important. Again, it is assumed that the background can be measured from real data after variations of cuts have been performed. In the evaluation of the signal significance, it is assumed that after normalization of the $Z \to \tau\tau$ background at the Z-peak, the total background in the mass window is known with an uncertainty of ± 10 %.

A comparison between the predictions from the PYTHIA parton-shower Monte Carlo and the explicit matrix element calculations has been performed also for the dominant $Z + jet$ background. In PYTHIA, only diagrams with one hard jet ($q\bar{q} \to g\tau\tau$ and $qg \to q\tau\tau$) are available. A second jet, if present, arises from initial- or final-state radiation and is softer than jets obtained from a matrix element evaluation of the QCD Zjj process. Studies have shown [14,30] that QCD Zjj events produced with matrix element calculations yield a background contribution, which is about a factor of two larger than the PYTHIA estimate. Therefore, the more conservative estimate has been used in the evaluation of the signal significance.

6.4 Discovery potential as a function of mass

The analyses outlined above has been performed for Higgs boson masses in the range from 110 to 150 GeV/c^2. The expected numbers of signal and background events and the statistical significance for a Higgs boson discovery expressed in terms of Gaussian standard deviations are given in Table 10 for an integrated luminosity of 30 fb^{-1} for the three τ decay channels considered, as well as for the combination of all channels. As described above, an uncertainty of ±10% on the background is assumed. After combination of all channels, an observation of a Higgs boson in the $\tau\tau$ decay mode looks feasible over the mass range from 115 to 140 GeV/c^2 with an integrated luminosity of 30 fb^{-1}.

The number of signal and background events in the selected mass window is affected by the $\tau\tau$ mass resolution, *e.g.*, if the mass resolution would be degraded from 12 to

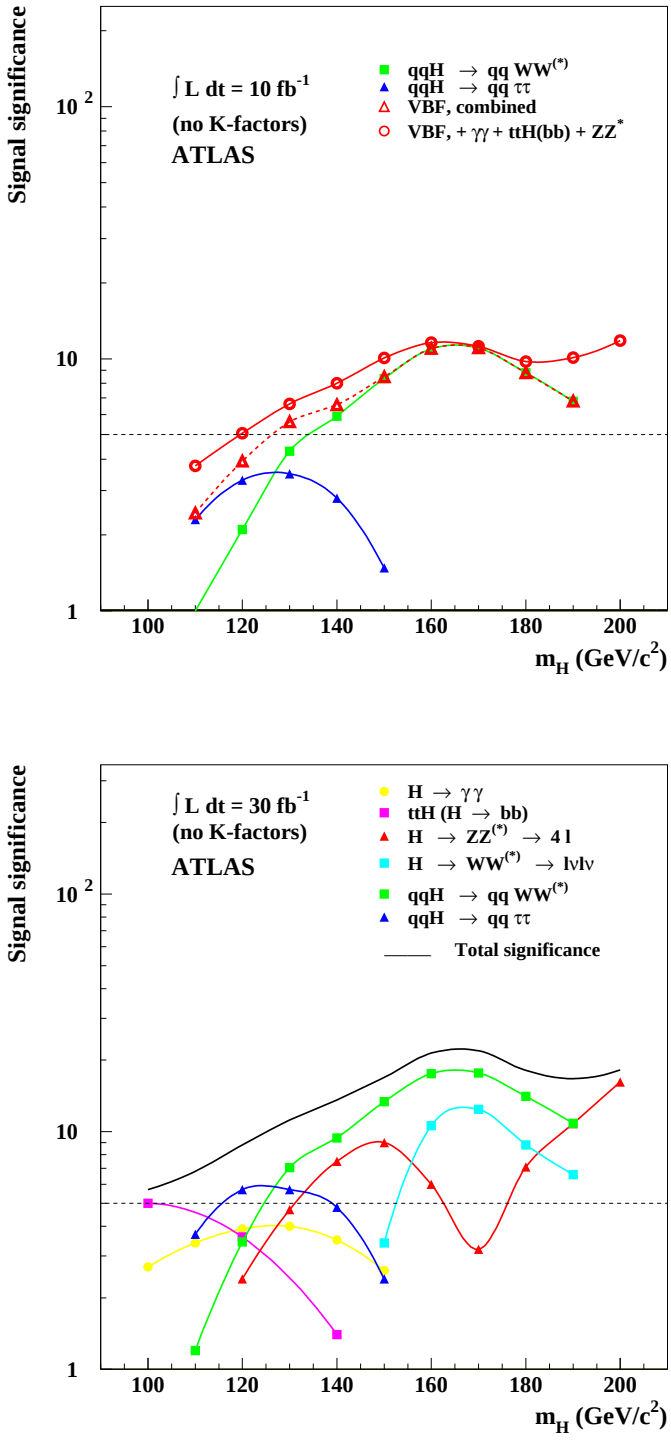

Fig. 13. *ATLAS sensitivity for the discovery of a Standard Model Higgs boson for integrated luminosities of 10 and 30* fb^{-1} *. The signal significances are plotted for individual channels, as well as for the combination of channels. A systematic uncertainty of* $\pm$ *10% on the background has been included for the vector boson fusion channels.*

m_H (GeV)	110	120	130	140	150
$H \to \tau\tau \to e\mu P_T^{miss}$					
Signal	9.7	8.4	6.3	3.8	1.8
Background	17.3	7.1	4.1	3.0	2.6
Stat. significance	1.9	2.5	2.3	1.7	0.7
$H \to \tau\tau \to ee/\mu\mu P_T^{miss}$					
Signal	9.7	8.3	6.3	3.8	1.8
Background	16.2	6.6	4.5	3.5	2.6
Stat. significance	1.9	2.6	2.3	1.5	0.7
$H \to \tau\tau \to \ell\ had\ P_T^{miss}$					
Signal	16.8	15.6	11.8	8.9	3.8
Background	31.9	7.7	3.6	2.5	2.5
Stat. significance	2.4	4.2	4.4	3.9	1.7
combined					
Stat. significance	3.7	5.7	5.7	4.8	2.4

Table 10. *Expected signal and background rates and statistical significance for the three $\tau\tau$ decay channels as a function of m_H assuming an integrated luminosity of 30* fb^{-1}.

15 GeV/c^2 the number of signal events for a Higgs boson with a mass of 120 GeV/c^2 in the $e\mu$-channel would be reduced from 8.4 to 6.8, whereas the number of background events would increase from 7.1 to 10.4.

7 The ATLAS Higgs boson discovery potential

The ATLAS Higgs boson discovery potential in the mass range 110 - 190 GeV/c^2 including the vector boson fusion channels discussed here is shown in Fig. 13 for integrated luminosities of 10 and 30 fb^{-1}. The vector boson fusion channels provide a large discovery potential even for small integrated luminosities. Combining the two vector boson fusion channels, a Standard Model Higgs boson can be discovered with a significance above 5 σ in the mass range 135 to 190 GeV/c^2 assuming an integrated luminosity of 10 fb^{-1} and a systematic uncertainty of 10% on the background. If the vector boson fusion channels are combined with the standard Higgs boson discovery channels [1] $H \to \gamma\gamma$, $H \to ZZ^{(*)} \to 4\ell$, and $t\bar{t}H$ with $H \to b\bar{b}$, the 5 σ discovery range can be extended down to ∼120 GeV/c^2.

For an integrated luminosity of 30 fb^{-1}, the full mass range can be covered by ATLAS with a significance exceeding 5σ. Over the full mass range several channels will be available for a Higgs boson discovery. The various discovery channels are complementary both from physics and detector aspects. The three different channels test three different production mechanisms, the gluon-gluon fusion via the $\gamma\gamma$ channnel, the vector boson fusion via the channels discussed here and the associated $t\bar{t}H$ production via the $t\bar{t}H$ with $H \to b\bar{b}$ mode. This complementarity also provides sensitivity to non-standard Higgs models, such as fermiophobic models [33].

Also different detector components are essential for the different channels. The $H \to \gamma\gamma$ decays require excellent electromagnetic calorimetry. In the identification of the vector boson fusion the measurement of jets, in particular the reconstruction of the forward tag jets is essential. The Higgs detection in $b\bar{b}$ decays via the associated $t\bar{t}H$ production relies to a large extent on the excellent b-tagging performance of the ATLAS Inner Detector.

8 Conclusions

The discovery potential for the Standard Model Higgs boson in the mass range below 190 GeV/c^2 has been studied using the vector boson fusion process. It has been demonstrated that the ATLAS experiment has a large discovery potential in the $H \to WW^{(*)} \to \ell^+\ell^- P_T^{miss}$ channel. The additional signatures of tag jets in the forward region and of a low jet activity in the central region of the detector allow for a significant background rejection, such that a better signal-to-background ratio than in the inclusive $H \to WW^{(*)}$ channel, which is dominated by the gluon-gluon fusion process, is obtained. As a consequence, the signal sensitivity is less affected by systematic uncertainties in the predictions of the background levels. The present study shows that the ATLAS experiment at the LHC would be sensitive to a Standard Model Higgs boson in this decay channel in the mass range between ∼135 and 190 GeV/c^2 with data corresponding to an integrated luminosity of only 10 fb^{-1}.

In addition, it has been shown that in the mass region $m_H < 140$ GeV/c^2, the ATLAS experiment is also sensitive to the $\tau\tau$ decay mode of the Standard Model Higgs boson in the vector boson fusion channel. A discovery in this final state would require an integrated luminosity of about 30 fb^{-1}. The detection of the τ decay mode is particularly important for a measurement of the Higgs boson couplings to fermions.

The present study confirms that the search for vector boson fusion at the LHC has a large discovery potential over the full range from the lower limit set by the LEP experiments up to $2m_Z$, where the high sensitivity $H \to ZZ \to 4\ \ell$ channel takes over.

Acknowledgements

This work has been performed within the ATLAS Collaboration, and we thank collaboration members for helpful discussions. We have made use of the physics analysis

framework and tools which are the result of collaboration wide efforts. We would like to thank D. Zeppenfeld, D. Rainwater, T. Plehn and F. Gianotti for very useful discussions.

References

1. ATLAS Collaboration, *Detector and Physics Performance Technical Design Report*, CERN/LHCC/99-14 (1999).
2. CMS Collaboration, *CMS Technical proposal*, CERN/LHCC 94-38, CERN (1994).
3. LEP Collaborations, CERN-EP/2001-055 (2001), hep-ex/0107029.
4. D.L.Rainwater and D.Zeppenfeld, J. High Energy Phys. 12 (1997) 5, hep-ph/9712271.
5. D.L.Rainwater and D.Zeppenfeld, Phys. Rev. D60 (1999) 113004, hep-ph/9906218.
6. D.L.Rainwater, D.Zeppenfeld, K.Hagiwara, Phys. Rev. D59 (1999) 14037, hep-ph/9808468; T.Plehn, D.L.Rainwater and D.Zeppenfeld, Phys. Rev. D61 (2000) 093005.
7. M.Spira, VV2H programme, home.cern.ch/m/mspira-/www/proglist.html.
8. T.Han, G.Valencia and S.Willenbrock, Phys. Rev. Lett. 69 (1992) 3274.
9. M.Spira et al., Comp. Phys. Comm. 108 (1998).
10. H.L.Lai et al., Eur. Phys. J. C12 (2000) 375.
11. V.Cavasinni, D.Costanzo, *Search for $WH \to WWW \to \ell\nu\ell\nu$ jet jet*, ATLAS internal note ATL-PHYS-2000-013 (2000);
    D.Cavalli, *Combined analysis of $A \to \tau\tau$ events from direct and associated bbA production*, ATLAS internal note ATL-PHYS-2000-005 (2000).
12. T.Sjöstrand, Comp. Phys. Comm. 82 (1994).
13. S.Jadach, Z.Was, CERN-TH-6793 (1993).
14. G.Azuelos and R.Mazini, *Searching for $H \to \tau\tau \to \ell\nu\nu$ + hX by vector boson fusion in ATLAS*, ATLAS internal note ATL-PHYS-2003-004 (2003).
15. ONETOP Monte Carlo programme, http://www.pa.msu.edu/brock/atlas-1top/EW-top-programs.html.
16. A.Pukhov et al., hep-ph/9908288.
17. E.Richter-Was, D.Froidevaux, L.Poggioli, *ATLFAST 2.0, a fast simulation package for ATLAS*, ATLAS internal note ATL-PHYS-98-131 (1998).
18. ATLAS Collaboration, CERN/LHCC/2000-17 (2000).
19. D.Cavalli and S.Resconi, *Tau-jet separation in the ATLAS detector*, ATLAS internal note ATL-PHYS-98-118 (1998).
20. C.Buttar, R.Harper, and K.Jakobs, *Weak boson fusion $H \to WW^{(*)} \to \ell\nu\ell\nu$ as a search mode for an intermediate mass Standard Model Higgs boson at ATLAS*, ATLAS internal note ATL-PHYS-2002-033 (2002).
21. V.Cavasinni, D.Costanzo, I.Vivarelli, *Forward tagging and jet-veto studies for Higgs events produced via vector boson fusion*, ATLAS internal note ATL-PHYS-2002-008 (2002).
22. M.Dittmar and H.Dreiner, Phys. Rev. D55 (1997) 167.
23. K.Cranmer, P.McNamara, B.Mellado, W.Quayle, Sau Lan Wu, *Search for Higgs bosons decay $H \to WW^{(*)} \to \ell^+\ell^- P_T^{miss}$ for $115 < M_H < 130$ GeV using vector boson fusion*, ATLAS internal note ATL-PHYS-2003-002 (2003).
24. K.Jakobs and Th.Trefzger, *Standard Model Higgs boson search for $H \to WW^{(*)} \to \ell\nu\ell\nu$ with a mass between 150 and 190 GeV*, ATLAS internal note ATL-PHYS-2000-015 (2000).
25. V.Cavasinni, D.Costanzo, E.Mazzoni, I.Vivarelli, *Search for an intermediate mass Higgs boson produced via vector boson fusion in the channel $H \to WW^{(*)} \to \ell\nu$ jet jet*, ATLAS internal note ATL-PHYS-2002-010 (2002).
26. F.A.Berends, W.T.Giele, K.Kuijf, B.Tausk, Fermilab-Pub-90/213-T.
27. CDF Collaboration, F.Abe et al., Phys. Rev. Lett. 79 (1997) 4760.
28. D0 Collaboration, B.Abbott et al., Phys. Lett. B513 (2001) 292.
29. M.Klute, *A study of the weak boson fusion with $H \to \tau\tau$ and $\tau \to e(\mu)$*, ATLAS internal note ATL-PHYS-2002-018 (2002).
30. T.Takemoto, S.Asai, J.Kanzaki, R.Tanaka *Study of $H \to \tau\tau \to \ell$ had $+x$ via vector boson fusion in ATLAS*, ATLAS internal note ATL-COM-PHYS-2003-007 (2003).
31. K.Cranmer, B.Mellado, W.Quayle, Sau Lan Wu, *An update of the VBF $H \to \tau\tau \to \ell\ell$ cut analysis*, ATLAS internal note ATL-COM-PHYS-2003-002 (2003).
32. O.J.Eboli and D.Zeppenfeld, Phys. Lett. B495 (2000) 147.
33. see for example: L.Brücher, R.Santos, hep-ph/9907434, and references therein.